ELSEVIER

Journal of Fluids and Structures 21 (2005) 3–24

JOURNAL OF FLUIDS AND STRUCTURES

www.elsevier.com/locate/jfs

Laboratory measurements of vortex-induced vibrations of a vertical tension riser in a stepped current

J.R. Chaplin[a,*], P.W. Bearman[b], F.J. Huera Huarte[b], R.J. Pattenden[a]

[a]*School of Civil Engineering and the Environment, University of Southampton, Highfield, Southampton SO17 1BJ, UK*
[b]*Department of Aeronautics, Imperial College of Science, Technology & Medicine, Prince Consort Road, London SW7 2BY, UK*

Received 2 November 2004; accepted 21 April 2005

Abstract

This paper describes measurements of the vortex-induced vibrations of a model vertical tension riser in a stepped current. The riser, 28 mm in diameter, 13.12 m long and with a mass ratio (mass/displaced mass) of 3.0, was tested in conditions in which the lower 45% was exposed to a uniform current at speeds up to 1 m/s, while the upper part was in still water. Its response in the in-line and cross-flow directions was inferred from measurements of bending strains at 32 equally spaced points along its length. Cross-flow vibrations were observed at modes up to the 8th, with standard deviations of individual modal weights greater than 50% of the riser's diameter. Except at the lowest reduced velocities, the response included significant contributions from several modes, all at a frequency controlled by lock-in of the dominant mode. In the presence of multi-mode responses, drag coefficients were up to 120% greater than those for a stationary cylinder at the same Reynolds numbers, and like overall measures of in-line and cross-flow displacements, revealed a strong dependence on the modal composition of the motion.

Keywords: Vortex-induced vibration; Riser; Vortex shedding; Nonuniform current; Multi-mode response; Drag

1. Introduction

Modelling the vortex-induced vibrations of a vertical tension riser under realistic conditions in a nonuniform current in the laboratory is experimentally rather difficult, and has scarcely ever been achieved. Key features of offshore risers are that they have length-to-diameter ratios of the order of at least 10^3, and that they undergo vibrations in high modes where the frequency intervals between adjacent modes are proportionately very small. Nevertheless, the ratio of the wavelength of any excited mode to the diameter of the riser is likely to be of order 10^2. Taken together with the experimental needs of avoiding the effects of low Reynolds numbers, of measuring the riser's response nonintrusively, and of having a controllable and well-documented incident flow, these features have restricted progress towards an understanding of the multi-mode response of risers to vortex excitation. Also, the inherently large-scale three-dimensional nature of the flow has inhibited advances towards reliable predictions based on computational fluid dynamics. The purpose of the work described in this paper was to improve our knowledge of the physics of vortex-induced vibrations of risers, and to provide reliable and well-documented data to support the development of predictive models.

*Corresponding author. Tel.: +44 23 8059 2843; fax: +44 23 8067 7519.
E-mail address: j.r.chaplin@soton.ac.uk (J.R. Chaplin).

0889-9746/$ - see front matter © 2005 Elsevier Ltd. All rights reserved.
doi:10.1016/j.jfluidstructs.2005.04.010

In respect of viscous effects, there is some evidence to suggest that in any experiment designed to have some quantitative similarity with conditions in the field, the Reynolds number should be kept above a few thousand. Close agreement has been found between measurements of the in-line vortex-induced response of an elastically mounted cylinder in this range and those from large scale measurements at Reynolds numbers of order 10^5 (Johanning et al., 2001). Secondly, it seems reasonable that a model riser's aspect ratio should not be much less than about 500, in order to preserve a representative ratio between the wavelength of higher modes and its diameter. These factors suggest that, in a current of around 1 m/s, its diameter should not be less than about 20 mm, and its vertical length should be at least 10 m. Such an experiment demands unusual facilities.

The previous investigation that most closely resembles the experiments described below seems to be that of Lie et al. (1997, 1998), in which the model riser (diameter 20 mm, total length 12.6 m) could be inclined to the vertical in a radial plane in a rig that rotated around its central axis at constant speed. The riser was thus exposed to a current with an adjustable degree of shear, and its cross-flow motion was measured with nine internal accelerometers during the first rotation into water initially at rest. The measured cross-flow response contained contributions from several modes, all at a single frequency. For a given average velocity over the length of the riser, the average root-mean-square displacement and the peak frequency were not sensitive to the degree of shear in the current.

The present paper describes an experimental project in which a vertical model riser, 28 mm in diameter, 13.12 m long, was exposed to a stepped current consisting of a uniform flow of up to 1 m/s over almost half of its length. The remainder of the riser was in still water. Measurements were obtained of the riser's response to vortex excitation at modes up to the 8th in transverse vibrations, and up to the 14th in the in-line direction. Considerable progress has been made in understanding these measurements since a preliminary analysis of them was described by Chaplin et al. (2004a). Before that publication, blind predictions of the model riser's displacements and curvatures had been carried out with 11 different codes. Some of these were presented by Chaplin et al. (2004b); they appear in a more complete form in Chaplin et al. (2005).

2. Experimental arrangements

2.1. The riser and its installation

The experiments were carried out at Delft Hydraulics in the Delta Flume, which was used as a towing tank. The flume is 230 m long, 5 m wide and, in these tests, the water depth was 6.5 m. It is equipped with a heavy carriage whose maximum speed in either direction is 1.0 m/s. The overall layout of the experiments is shown in Fig. 1.

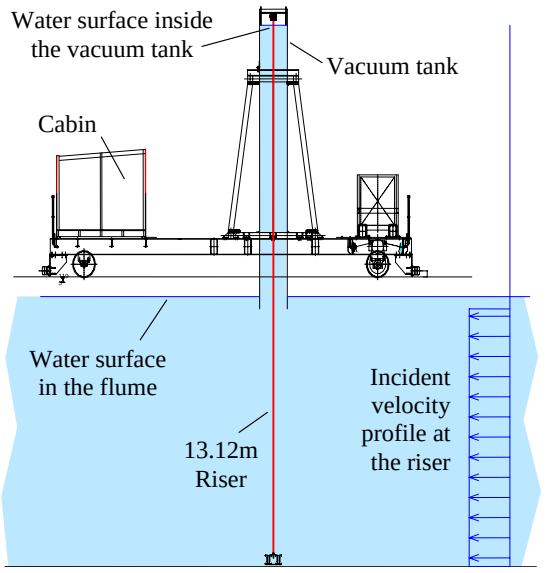

Fig. 1. Layout of the experiments. The supporting structure for the bottom of the riser is not shown.

The riser passed through the depth of water in the flume and up to the top of a tank (the 'vacuum tank') which was open at the bottom at an elevation just below the surrounding water surface in the flume. The vacuum tank was otherwise sealed and during the experiments it was almost filled with water by evacuating air from the top. When the carriage was moving, the riser thus experienced a stepped current consisting of uniform flow over its lower part and still water elsewhere, as shown in Fig. 1.

A large steelwork construction was built on to the carriage, to provide a stiff mounting point for the bottom of the riser (at an elevation of 360 mm above the floor of the flume), and to support the vacuum tank (0.8 m × 0.3 m in plan), which was 7.54 m high. The submerged part of the substructure was all downstream of the riser during the tests, which were carried out by driving the carriage in always the same direction along the flume.

The model riser consisted of a phosphor-bronze spine inside a fluoroplastic tube of wall thickness 0.5 mm and outer diameter 28 mm. The spine was machined from solid bars in 820 mm long sections into a core rod of 8 mm diameter, with 3 mm thick integral circular fins of diameter 27 mm at intervals of 9 mm. The fins supported the outer tube and had cut-outs to accommodate electrical cables. Strain gauges were installed on flats machined into the 8 mm circular core at intervals of 410 mm over its entire length to measure its curvature about two axes, in a total of 64 half-bridges. Also, three miniature accelerometers were fitted inside the riser to provide checks on displacements obtained from the strain gauge signals. Fig. 2 shows part of the assembled riser, including a strain gauge station, two of the accelerometers and the associated cables—16 of which emerged from each end of the riser. Prior to installation, the 16 identical sections of the riser were connected together with machined joints that were filled with epoxy to prevent any relative movement. The overall length of the riser was 13.12 m and during the experiments, it was internally flooded. The installation on the carriage is shown in Fig. 3.

The riser was installed with universal joints at each end and at the top it was suspended from a tensioning system. This consisted of a parallel array of extension springs connected between the universal joint and an upper beam whose elevation could be adjusted from outside the vacuum tank. The springs also ensured that the riser's tensile limit was never exceeded by the increase in loading associated with drag.

The principal instrumentation is listed in Table 1, referring to in-line (IL) and cross-flow (CF) directions. Accelerometers were installed to monitor the horizontal motion of the riser's mounting points at top and bottom. During the tests they recorded accelerations over a wide range of frequencies, but with no dominant components at the riser's frequencies of vibration. Typical values of corresponding root-mean-square displacements within a range of frequencies between 0.5 and 4 times the Strouhal shedding frequency were less than 1 mm at carriage speeds up to 0.7 m/s, and less than 2.5 mm at 1 m/s.

2.2. Calibrations, data processing, test conditions

The 64 strain gauge circuits were calibrated before the riser sections were joined together, and this was done by loading each 820 mm long element of the riser in turn at mid-span when simply supported at its ends. In all cases the calibrations revealed a high degree of linearity and repeatability.

Once assembled and installed on the carriage, the in-line and cross-flow deflections of the riser from its initial vertical straight-line condition, denoted by $x(z,t)$ and $y(z,t)$, respectively, could be estimated by double numerical integration of the measured curvatures with respect to the elevation z (measured from the bottom of the riser). Boundary conditions are provided by the known (usually zero) displacements, and zero curvatures, at each end.

The deflected shape of the riser can be usefully represented in spectral terms, and for this purpose mode shapes are identified as $\varphi_n(z) = \sin nkz$, where $k = \pi/L$, and L is the riser's length. The displacements in in-line and cross-flow directions can then be expressed in terms of time-dependent modal weights u and v:

$$x(z,t) = \sum_{n=1}^{N} u_n(t)\varphi_n(z), \quad y(z,t) = \sum_{n=1}^{N} v_n(t)\ \varphi_n(z) \quad \text{with } N \leqslant 32. \tag{1}$$

An alternative procedure is to perform the spatial frequency analysis directly over each sequence of 32 measured curvatures to compute the modal weights from

$$x''(z,t) = k^2 \sum_{n=1}^{N} n^2 u_n(t)\varphi_n(z), \quad y''(z,t) = k^2 \sum_{n=1}^{N} n^2 v_n(t)\varphi_n(z), \tag{2}$$

where a prime denotes differentiation with respect to z.

A third approach (Lie and Kaasen, 2004) is to fit the measured curvatures to the forms of Eq. (2) with a least-squares procedure, including only certain modes. For a given set of conditions, all three methods were found to yield essentially identical results.

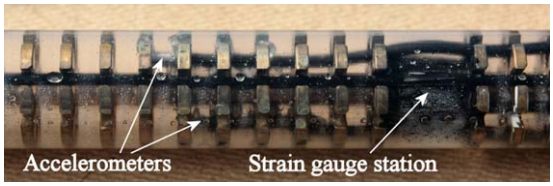

Fig. 2. Part of the model riser.

Fig. 3. The vacuum tank (with the riser beneath) mounted on the carriage.

Table 1
Instrumentation. A total of 86 channels of data were collected at 200 Hz

At the top of the riser	Tension load cell Drag load cell Frame accelerometers (IL, CF)
In the riser	32 strain gauge stations (IL, CF) 3 accelerometers (IL or CF)
At the bottom of the riser	Tension load cell Drag load cell Frame accelerometers (IL, CF) Excitation system and displacement feedback (CF)

Table 2
Experimental conditions; still-water top tensions and natural frequencies

Series	Top tension in still water (N)	Number of runs	Symbol	Frequencies of the first 7 modes measured in still water (Hz)						
A	389	19	+	0.405	0.873	1.326	1.804	2.278	2.797	3.389
B	813	77	◇	0.633	1.329	1.954	2.625	3.312	4.028	4.753
C	1185	11	□	0.782	1.423	2.394	3.203	4.024	4.875	5.704
D	1546	15	○	0.899	1.815	2.741	3.614	4.561	5.525	6.439
E	1925	16	△	1.037	2.046	3.084	4.099	5.127	6.222	7.298

All of these procedures require that x'' (for example) is an adequate approximation to the actual curvature $x''/(1+x'^2)^{3/2}$ of the curve $x(z)$. Numerical checks showed that in the present case the difference was very small indeed. The integration procedure is also based on the assumption that normals to the material faces on which the strain gauges were placed did not depart significantly from their orientations in the initial undeformed straight line case (namely the x and y directions). This issue is addressed in Appendix A, which concludes that the associated uncertainty in modal weights is likely to be at most two or three percent of one diameter. A third point to be considered in the data processing is that for a given modal displacement amplitude, the magnitude of the bending strain associated with the nth mode is proportional to n^2. Consequently when several modes are present, considerably more uncertainty must be attached to estimates of the lowest modes than to the highest. Appendix B shows that for this reason the lowest modes of displacement could not always reliably be obtained from the curvature measurements. Therefore, in computing displacements from the strain gauge results, the contribution of the first mode was included only when the standard deviation of curvature associated with it exceeded 3% of that of all modes combined. This procedure ensured that when, at low speeds, the first mode was the dominant one, it would not be omitted from the computed response. In the in-line direction (where bending strains were of a similar magnitude but generally concentrated in higher modes), comparisons with measured accelerations showed also that sometimes computed modes beyond the first were also unreliable and (as described in Appendix B) their contributions were then removed from the analysis. This procedure was applied only to the unsteady components of the measured curvatures; the computed time-averaged in-line offset of the riser at the elevation of the bottom of the vacuum tank was checked by visual observation during the tests, and was found to be very reliable.

The experiments were carried out in five series with still-water top tensions between 389 and 1925 N. The riser's natural frequencies in air and in still water were measured by driving it with a ramped frequency signal through an excitation system at the bottom. The first few of these frequencies, and the still-water top tensions used in each series of tests at carriage speeds up to 1 m/s, are set out in Table 2. The mass ratio of the riser (mass/displaced mass) including the mass of the internal water was 3.0, its submerged weight was 12.1 N/m, its bending stiffness was 29.9 N m^2 and its structural damping measured in free decay tests in air was 0.33%.

In each test the carriage was accelerated to a constant speed and measurements were made over a period of 60 s. In most cases, the interval between the end of one test and the start of the next was at least 15 min. Reynolds numbers were in the range 2500–25 000.

3. Discussion of experimental results

The coordinates of a point on the riser are identified as $(x(z,t), y(z,t))$. Overall indications of the magnitudes of in-line and cross-flow responses are provided by the standard deviations with respect to time of the standard deviations of x and y over z. These are defined by

$$\sigma_x = \sqrt{\frac{1}{T}\int_0^T \frac{1}{L}\int_0^L [x(z,t) - \bar{x}(z)]^2 \,\mathrm{d}z\,\mathrm{d}t}, \quad \sigma_y = \sqrt{\frac{1}{T}\int_0^T \frac{1}{L}\int_0^L y(z,t)^2 \,\mathrm{d}z\,\mathrm{d}t}, \tag{3}$$

where $\bar{x}(z)$ is the time-averaged in-line displacement. (In the case of an oscillation in a pure mode of the form $x = a\sin(n\pi z/L)\cos(m\omega t)$, the value of σ_x would be $a/2$.) The integration in time is carried out over an interval T in which the velocity was constant; generally this was the last 30 s of the 60 s duration of each test. Standard deviations of the in-line and cross-flow curvatures σ_{cx} and σ_{cy} are defined in the same way.

These results are plotted in Fig. 4 as functions of the reduced velocity $U/f_1 d$, where U is the flow velocity, and d the cylinder diameter. The frequency f_1 is an estimate of the riser's natural frequency in still water in the fundamental mode, at the mean tension observed during each test. The tension increases with the velocity owing to the mean in-line offset that is generated by drag, and the corresponding frequency was interpolated in each case from the results of tests carried out in still water over a range of tensions.

In Figs. 4(a) and (b) the standard deviations of displacements appear to be quite widely scattered, with most points in the range 0.06 and 0.12 diameters for in-line motion, and between 0.25 and 0.4 diameters for the cross-flow direction. However, as will be seen below, this is a consequence of systematic changes that take place as the reduced velocity passes through the lock-in range for successive modes.

The in-line and cross-flow curvatures (Figs. 4(c) and (d)) are of similar magnitudes. The fact that the curvatures increase approximately with $(U/f_1 d)^2$ is consistent with the interpretation that the oscillations occur at an approximately constant amplitude, at a mode number that increases linearly with reduced velocity.

Typical instantaneous deflected shapes of the riser are shown in Fig. 5, where in-line and cross-flow displacements are plotted against the relative elevation z/L. The time-averaged in-line displacement (plotted on the left) reflects the effect of the drag on the lower part of the riser (where it is exposed to a steady current over the region identified by a vertical bar), while the upper part (in still water) follows a straight line as expected. Continuous lines in Figs. 5(b) and (c) plot the positions of the riser (measured from the mean in the case of Fig. 5(b)) at intervals of 0.015 s through one period (0.201 s) of the cross-flow oscillation, starting 20 s after the first movement of the carriage into still water. Broken lines show the envelopes of in-line and cross-flow displacements recorded over the next 40 s, or 200 cross-flow oscillations.

A typical feature of the results, demonstrated in Fig. 5, is that displacements of the upper part of the riser (in still water) were no smaller than those exposed to the current below. It is also worth noting that in this case there was a very high degree of periodicity over the entire duration of the test, as can be seen from the time series of modal weights for the same case shown in Fig. 6. In both in-line and cross-flow directions there is evidence of simultaneous contributions from modes on either side of the dominant ones, namely the 12th (in-line) and 7th (cross-flow). All those in the in-line direction have the same frequency, which is twice that of all the cross-flow modes, and which corresponds to a reduced velocity of 6.1. Evidence presented later suggests that the vortex excitation would have been locked-in at the frequency of the dominant mode, and this reduced velocity is typical of those at which maximum cross-flow responses of cylinders have been observed at similar Reynolds numbers (Sarpkaya, 2004).

In the absence of any knowledge of the distribution of added mass, and neglecting the effect of variations in tension, the mode shapes have been assumed to be sinusoids, as mentioned above. The fact that all contributing modes defined in this way are neither in phase nor in anti-phase with each other, as can be seen in Fig. 6—and the fact that there are no pure nodes in the profiles in Fig. 5—indicates that part of the motion in both directions is a travelling wave.

The strongly periodic nature of the motion seen in Figs. 5 and 6 was not observed in every case. In many, a steady state developed only after a period in which several modes exhibited continually changing amplitudes, as in Fig. 7. Between the conditions of Figs. 6 and 7 there was an increase in the carriage speed of 0.05 m/s, corresponding to an increase in the reduced velocity $U/f_1 d$ (allowing for the associated change in tension) of less than 0.7. Sometimes, mode switching as seen in Fig. 7 was triggered by a disturbance, such as vibration in the carriage due to irregularities in the rails, and on other occasions it occurred without apparent external influence.

For the conditions of Fig. 7, the riser's deflected shapes are shown in Fig. 8. Plots (b, in-line) and (c, cross-flow) refer to the time from $t = 20$ s (when the 8th mode was dominant), and (d) and (e) to that from $t = 40$ s, when the 6th mode had become established. As in Fig. 5, the dashed lines are the envelopes of the motion recorded over the remaining duration of the test. It is characteristic of such cases that, when switching from one mode to another, the riser would momentarily undergo large excursions. This can be seen in the envelopes plotted in Figs. 8(b) and (c) which extend beyond 0.6 diameters in-line and 1.4 diameters cross-flow. Another common feature of cases where there was not a single robust mode was the distinctive appearance (as in Fig. 8(e)) of a travelling wave, particularly in the lower part of the riser.

In Fig. 8(a) are plotted the time-averaged in-line displacements before (broken line) and after (continuous line) the change from mode 8 to mode 6 at about $t = 30$ s (Fig. 7). Clearly the establishment of a well-defined excitation regime corresponded to a significant increase in drag.

In a small number of cases, no steady state appeared but the vibrations continued with highly modulated amplitudes over the entire duration of the test (Fig. 9).

In the light of nonstationary response histories, of which Figs. 7–9 have provided examples, it may be misleading (for tests of short duration) to represent overall responses in terms of unconditional standard deviations (as in Fig. 4). These data were accordingly recalculated using as far as possible in each case an integration period T over which the motion was dominated by one or more cross-flow modes with almost constant amplitudes. Thus, in the case of Fig. 7, the integration was subsequently carried out over the period $40\,\text{s} < t < 60\,\text{s}$; in that of Fig. 9 over the period $25\,\text{s} < t < 38\,\text{s}$. Except where stated otherwise, all results presented below are conditioned in this way.

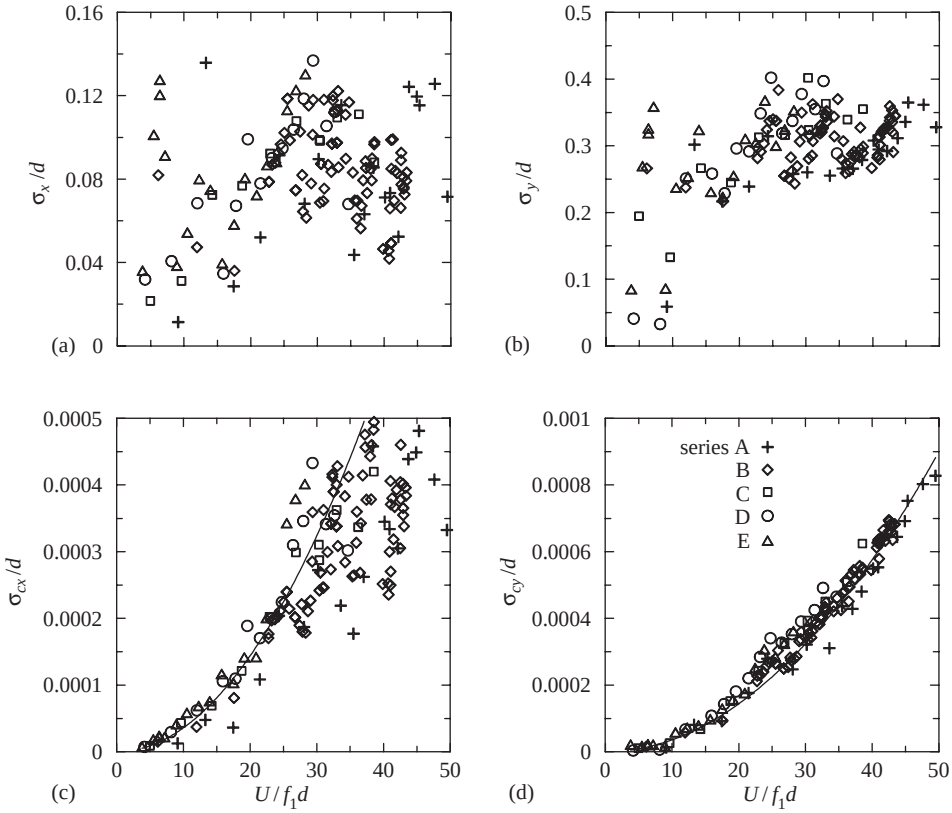

Fig. 4. Standard deviations of (a) in-line and (b) cross-flow displacements, and of (c) in-line and (d) cross-flow curvatures. The same quadratic curve $\sigma_c d = 3.6 \times 10^{-7}(U/f_1 d)^2$ is shown in (c) and (d).

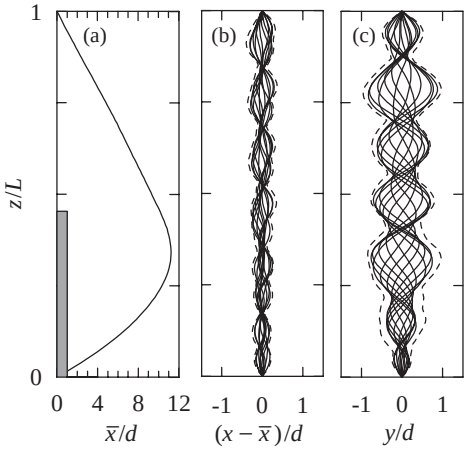

Fig. 5. Deflected shapes of the riser. (a) The mean in-line deflection. Instantaneous deflected shapes are shown at intervals of 0.015 s through one cross-flow oscillation as continuous lines in (b) for the in-line direction (measured from the mean), and (c) for the cross-flow direction. Broken lines represent the envelopes of the motion over a period of 40 s. Carriage speed = 0.85 m/s; top tension 939 N; $U/f_1 d = 47.1$; case 21_A016.

Overall responses are shown in Figs. 10 and 11 (in-line) and 12 and 13 (cross-flow). The data fall into clearly defined families that are identified by the combination of dominant in-line and cross-flow modes. In Figs. 10 and 12(a), data for modes 1–3 are plotted from all five test-series, but (for the sake of clarity) only those from

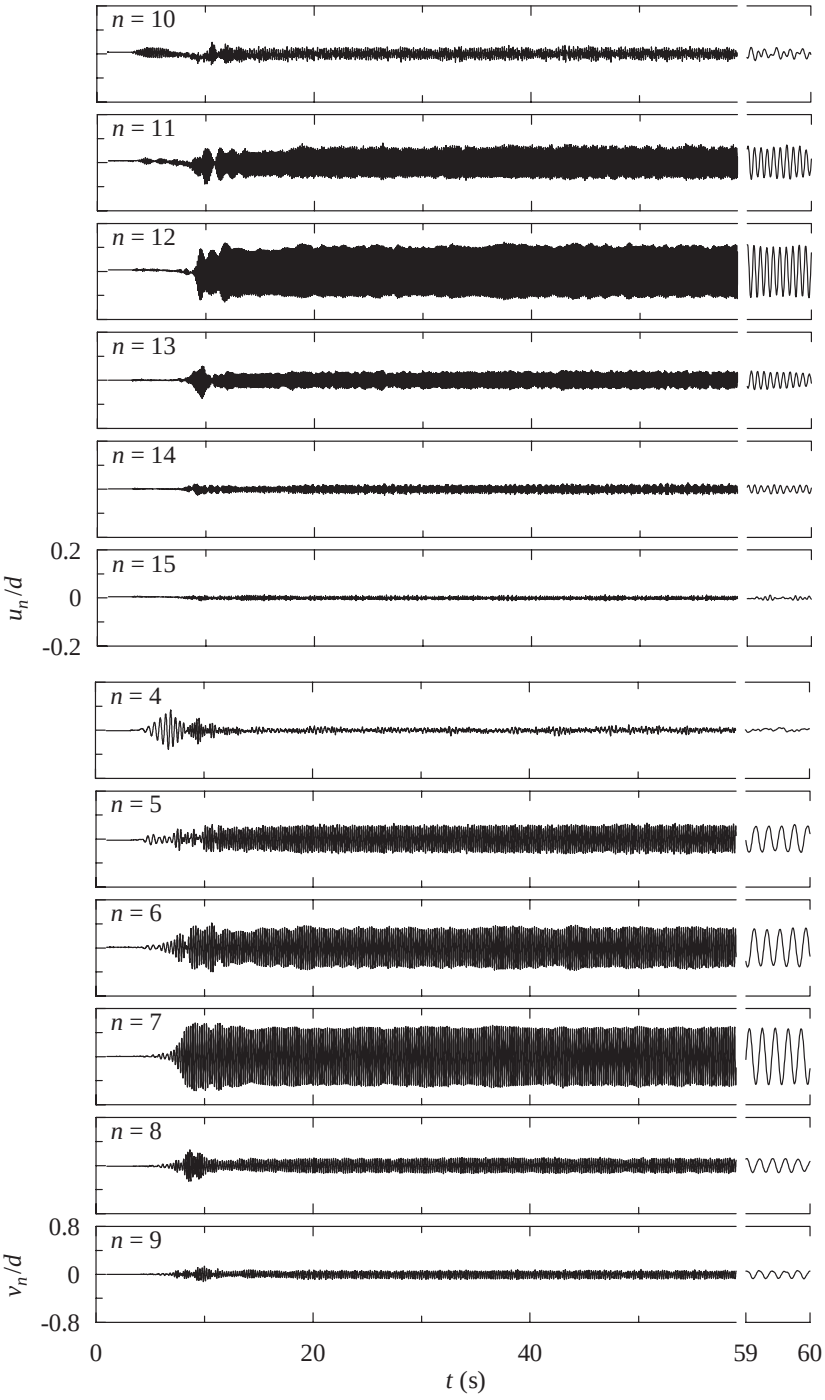

Fig. 6. Modal weights of in-line (above) and cross-flow (below) oscillations for the test case of Fig. 5. Vertical scales are the same for all graphs in each set. The last second of the run is shown over an expanded time scale.

series B are shown for the higher modes. The points omitted from Figs. 10 and 12 are shown in Figs. 11 and 13, respectively.

In each group, corresponding to a particular modal pattern, there is an increase in the cross-flow displacement with increasing reduced velocity, but there is no corresponding decrease. It should be noted that all

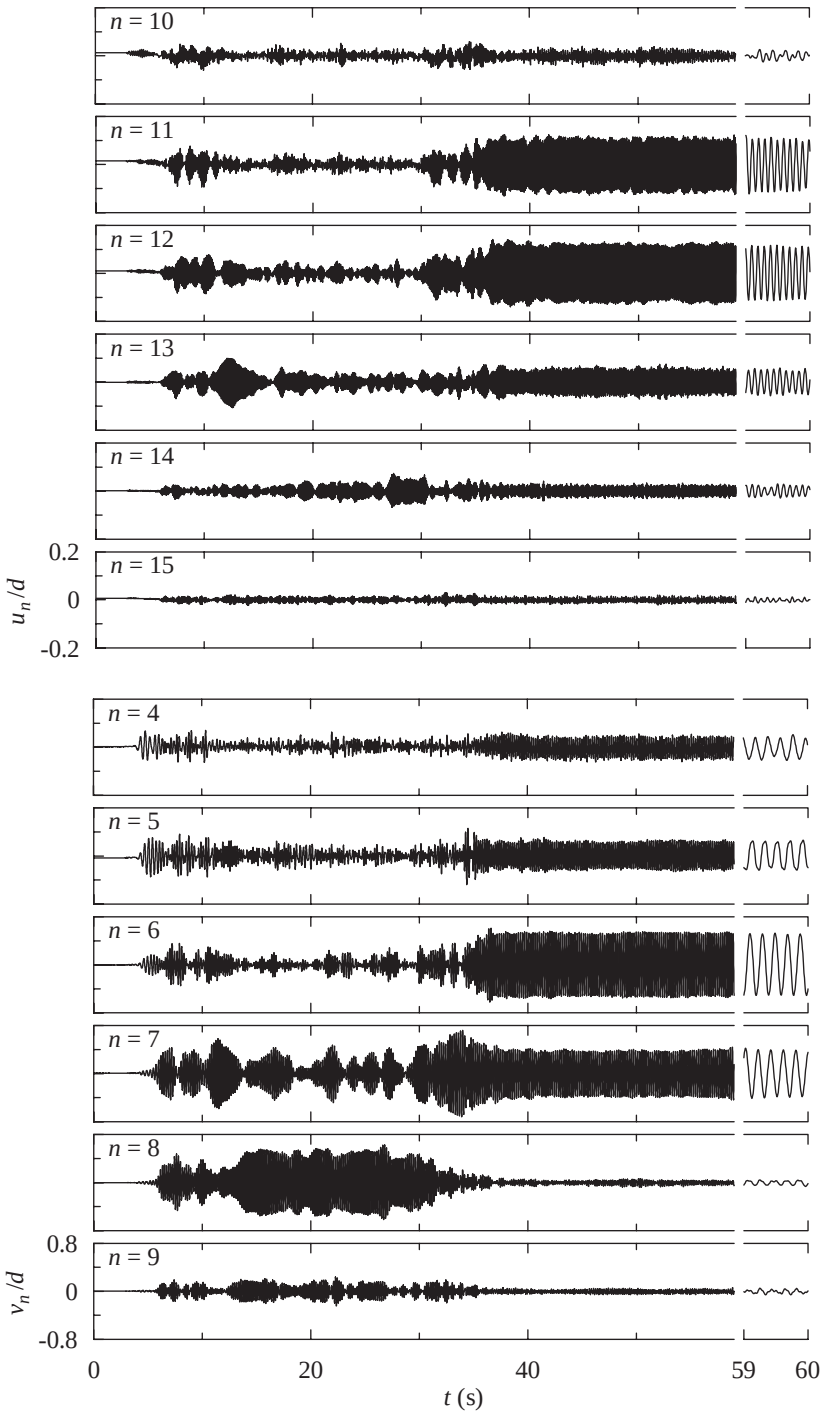

Fig. 7. Modal weights of in-line (above) and cross-flow (below) oscillations: carriage speed = 0.90 m/s; top tension 1073 N; $U/f_1 d = 47.8$; case 21_A017. Vertical scales are the same for all graphs in each set. The last second of the run is shown over an expanded time scale.

of these measurements were carried out after accelerating the carriage up to the test speed, so there was no opportunity for the vortex shedding to maintain a frequency normally associated with a higher reduced velocity, in a hysteretic fashion. Instead, as the reduced velocity is progressively increased, each subsequent modal pattern

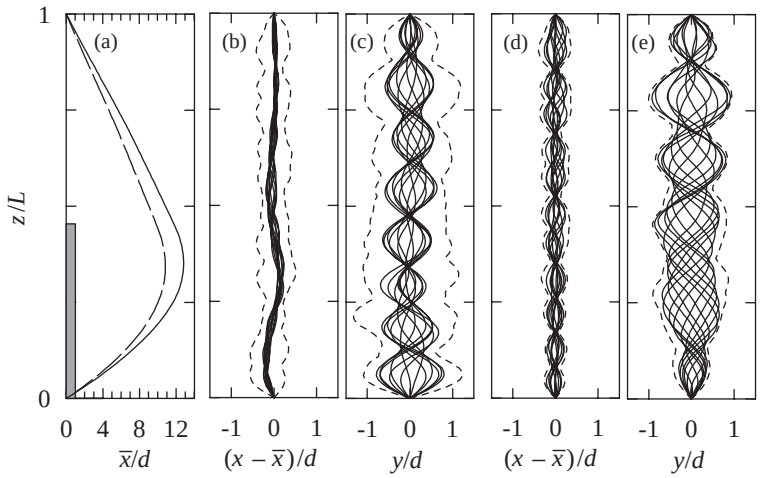

Fig. 8. Deflected shapes of the riser for the conditions of Fig. 7. (a) The mean in-line deflection, showing a step change resulting from the redistribution of modal responses that occurred at about $t = 30$ s (Fig. 7). The long-dashed line is the mean deflected shape over the interval $10\,\text{s} < t < 30\,\text{s}$; the continuous line is that over the interval $40\,\text{s} < t < 60\,\text{s}$. In (b–e) instantaneous deflected shapes are shown at intervals of 0.015 s through one cross-flow oscillation as continuous lines. In (b) and (c) the sequence starts at $t = 20$ s, and in (d) and (e) at 40 s. Broken lines in each case represent the envelopes of the motion over the remainder of the test of 60 s total duration.

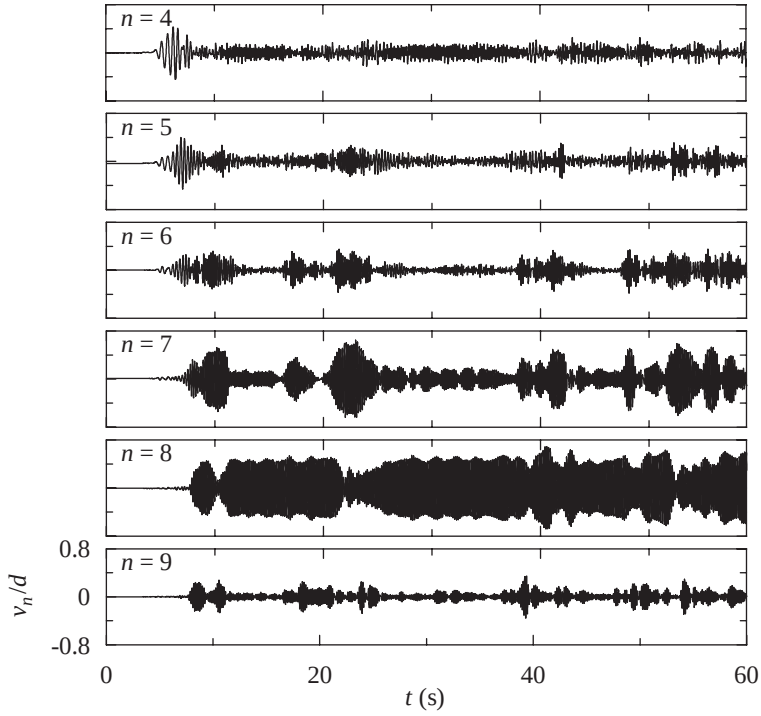

Fig. 9. Modal weights of cross-flow oscillations: carriage speed = 1.00 m/s; top tension 958 N; $U/f_1 d = 49.3$; case 21_A019. Vertical scales are the same for all graphs.

takes over with initially a much reduced amplitude. Among the higher modes in some cases there is considerable overlap.

Broken lines in Figs. 10 and 12(a) serve to identify the members of each group and are linear fits to all of the associated data points. The points that fall between the groups were generally from cases in which the modal weights

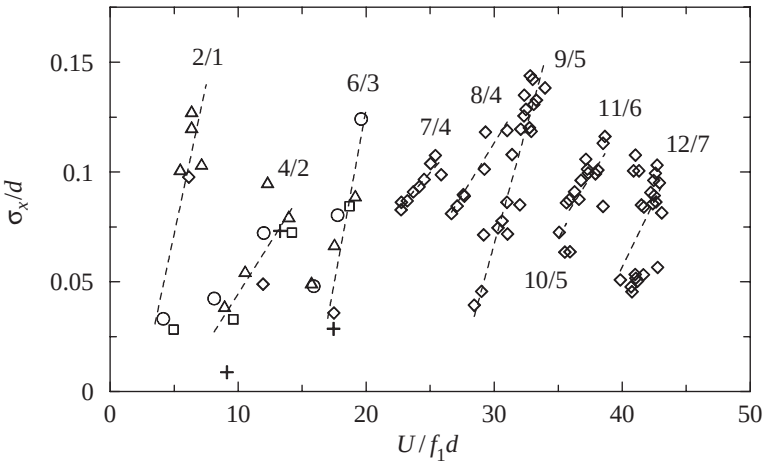

Fig. 10. Standard deviations of in-line displacements computed over time intervals in which the response was dominated by cross-flow modal contributions of almost constant amplitudes. Groups of points are identified by broken lines labelled with (dominant in-line mode)/(dominant cross-flow mode). Data from all test-series are plotted for modes up to the third cross-flow mode, thereafter the data are shown only for series B.

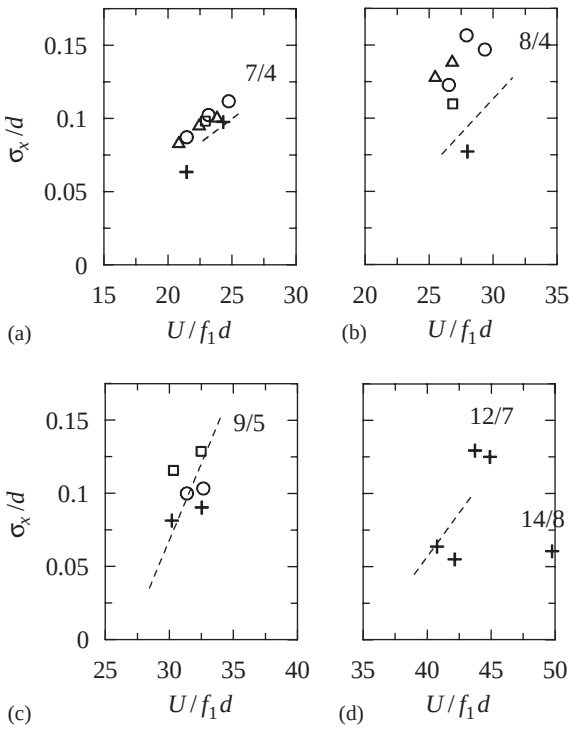

Fig. 11. In-line standard deviations for series other than B, above the third mode (not shown in Fig. 10). The dashed lines for each combination of dominant modes are the same as those plotted there.

exhibited considerable modulation, as shown for example by those plotted in Figs. 12(b)–(e). The corresponding point in Fig. 12(a) lies between those groups with dominant cross-flow modes 4 and 5 (and dominant in-line modes 8 and 9). On the other hand, modal weights plotted in Figs. 12(f)–(i) for a member of the first of these groups (at almost the same reduced velocity) have much more constant amplitudes. It is also interesting to note that a jump in the dominant in-line

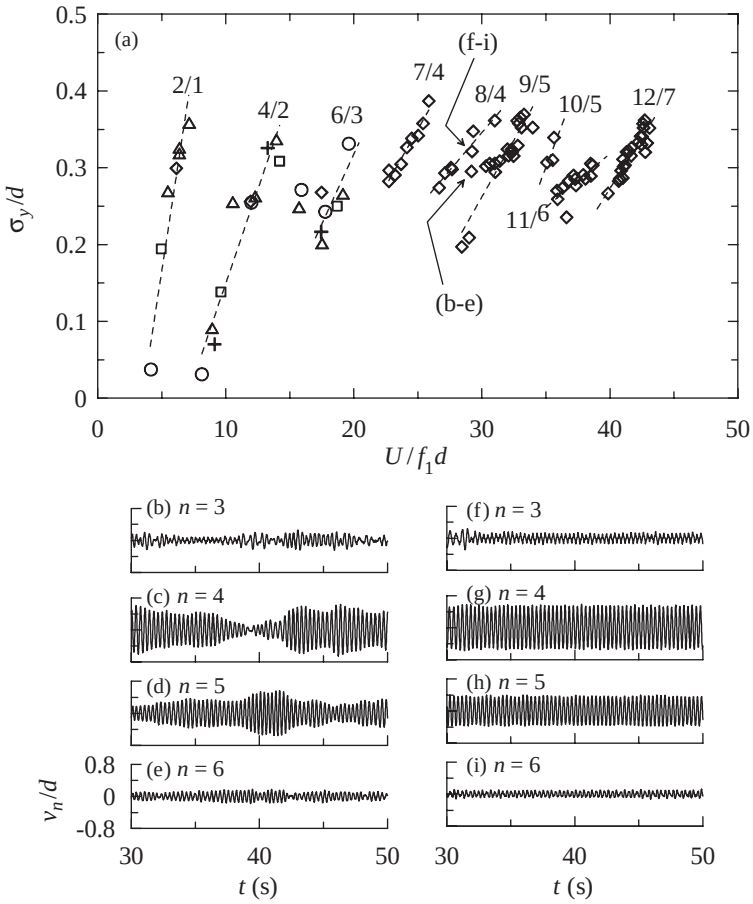

Fig. 12. (a) As for Fig. 10, for the cross-flow direction. Time series of modal weights for two neighbouring points identified in (a) are plotted below in (b–e) and (f–i).

mode (without any change in the dominant cross-flow mode) may be associated with step changes in the magnitude of the displacements in both directions. Examples are provided by the groups labelled 7/4 and 8/4, and those labelled 9/5 and 10/5, in Figs. 10 and 12.

Results for the higher modes from series A, C, D and E are plotted in Figs. 11 and 13. These follow trends similar to those established in Figs. 10 and 12(a), but at reduced velocities that are shifted down as the tension is increased and vice versa. The reduced velocities for all data points in these graphs are based on fundamental frequencies f_1 obtained at the appropriate tensions with the riser straight and vertical. The probable reason for the shifts in the points in Figs. 11 and 13 relative to those for the same modes in Figs. 10 and 12(a) is that the base frequencies for the former were not (and could not reliably be) adjusted to allow for the structural effect of the time-averaged in-line displacements. Finite element solutions suggested that this could lead to an increase in in-line modal frequencies by as much as 30%.

These results suggest that the modal content has a major effect on the overall amplitude of the riser's response, which is therefore quite sensitive to small changes in the reduced velocity.

The time-averaged displacement of the riser in the in-line direction followed the same form (Figs. 5(a) and 8(a)) in all cases. Increasing the speed of the carriage had the effect of increasing the drag, thereby increasing the tension P (as shown in Fig. 14(a)), the modal frequencies, and the maximum mean in-line offset $\bar{x}_{\max}$. The drag must be balanced by the sum of the horizontal components of tension at the ends of the riser, proportional to the product $\bar{x}_{\max}P$. Since the modal frequencies such as f_1 are approximately proportional to the square root of the tension, it follows that if the drag coefficient were constant, the maximum mean offset would be proportional to the square of the reduced velocity, $\bar{x}_{\max}/d = C\,(U/f_1d)^2$ with C independent of the initial still-water tension. Measurements of maximum mean offsets in all test-series, plotted together in Fig. 14(b), are clustered around this relationship, but depart from it by as much as

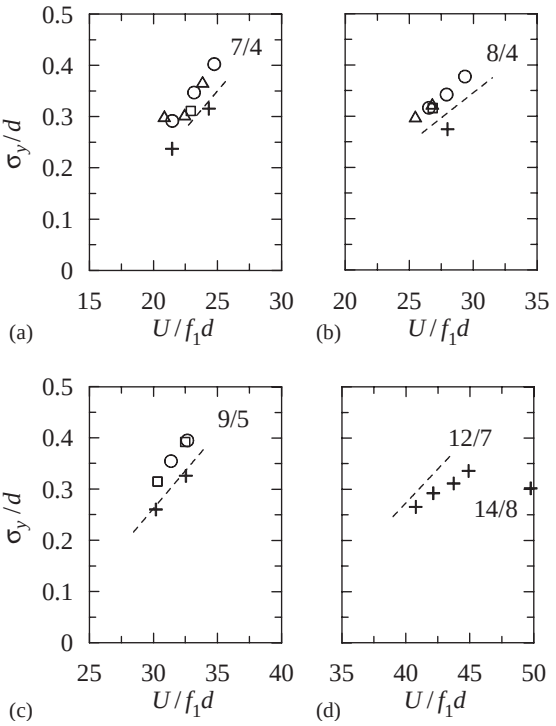

Fig. 13. Cross-flow standard deviations for series other than B, above the third mode (not shown in Fig. 12(a)). The dashed lines for each combination of dominant modes are the same as those plotted there.

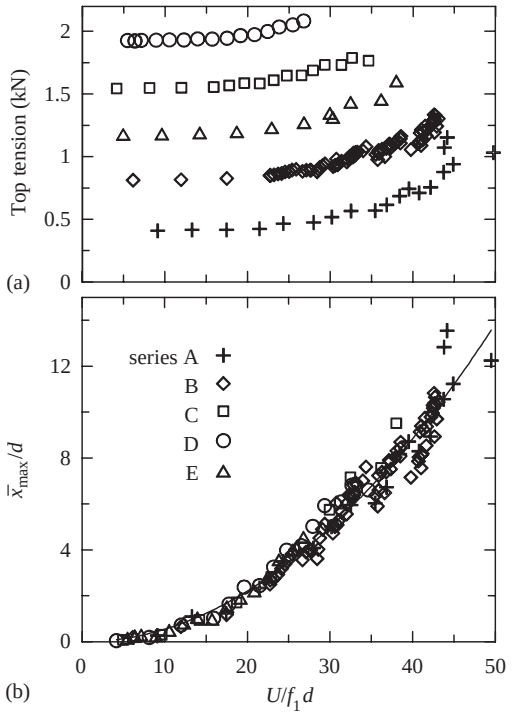

Fig. 14. (a) Top tensions and (b) maximum time-averaged in-line offsets from all test-series as functions of the reduced velocity. A continuous line in (b) is the best quadratic fit to all of the data.

20%, suggesting that there were significant changes in drag coefficients associated with mode switching (as mentioned above in connection with Fig. 8(a), and below).

Figs. 15(a) and 16(a) show the observed dominant frequencies f_x and f_y in the riser's in-line and cross-flow responses. These are normalized with respect to the estimated fundamental frequencies f_1 for the undeformed riser in still water, and advance mainly in a series of steps, indicating lock-in with an ascending sequence of modes as the reduced velocity increases. The steps do not occur at the same level in all test-series (particularly for the higher modes) probably because (as mentioned above) f_1 is not necessarily an appropriate reference frequency for those cases where the mean position of the riser is strongly deformed from a straight line. For this reason, and to avoid confusion, results from series C and D have been omitted from Figs. 15(a) and 16(a). In those series where the tests were carried out at closely spaced intervals of velocity, there is strong evidence of successive lock-in ranges centred around frequencies associated with a Strouhal number of 0.17.

Standard deviations of individual modal weights $\sigma_u^{(n)}$, $\sigma_v^{(n)}$ for all modes with significant levels of response are plotted in Figs. 15 and 16, showing the amplification of each one through its lock-in range. (Fig. 16(b) includes only points where the cross-flow first mode could be reliably identified, bearing in mind the criteria discussed in Appendix B.) As the centre of each lock-in range is approached, there is a monotonic increase in the amplitude of the respective mode. Generally a peak is reached before the previous mode has died away and after the next has begun. As the reduced velocity passes out of each lock-in range, the attenuation of the corresponding mode occurs not smoothly but in one or two broken rising sequences, often clearly linked to the growth of the next mode. At the highest reduced velocities the dominant cross-flow mode appears also in the in-line direction (Figs. 15(b)–(c)). Standard deviations of individual modes reached 0.16 diameters in-line and 0.53 diameters cross-flow.

The bottom plot in Fig. 16 shows mean drag coefficients computed from the horizontal component of end tensions. An alternative way of estimating drag coefficients was to compute, by means of a nonlinear finite element solution, the in-line displacement of the riser due to a uniformly distributed horizontal force acting over the region of the current. The drag coefficient was deduced from the magnitude of the force which gave the best match with the measured displacement. The two methods yielded almost identical results. Apart from a few points at low reduced velocities, where adjacent lock-in ranges do not overlap, these lie between 1.6 and 2.7. The drag coefficients reveal a strong dependence on the growth and attenuation of successive modes within each series.

An indication of the dependence of the drag coefficient on the amplitude of cross-flow motion is given in Fig. 17, which includes data from all test-series. In Fig. 17(a) drag coefficients are plotted as a function of σ_y, and are seen to be distributed around the line

$$C_d/C_{d0} = 1 + 2.3(\sigma_y/d) + 1.7(\sigma_y/d)^2, \tag{4}$$

where for each test C_{d0} is the drag coefficient for a stationary smooth cylinder in conditions of low free-stream turbulence at the same Reynolds number (Wieselsberger, 1921).

From field measurements of the drag of long vibrating cylinders over similar ranges of Reynolds numbers and participating modes, and at comparable length to diameter ratios, Vandiver (1983) proposed an equation of a different form:

$$C_d/C_{d0} = 1 + 1.043(2Y_{\text{r.m.s.}}/d)^{0.65}, \tag{5}$$

where $Y_{\text{r.m.s.}}$ is the root-mean-square cross-flow antinode displacement. This parameter was computed from the present measurements for the point on the riser (within the current) at which the peak-to-peak cross-flow motion was greatest, and the relative drag coefficients are plotted against $Y_{\text{r.m.s.}}/d$ in Fig. 17(b). The data points are rather more scattered when plotted in this way, but surround the dashed line which represents Eq. (5).

4. Conclusions

Comprehensive measurements have been made of the vortex-induced vibrations of a 13.12 m long model vertical tension riser of 28 mm diameter and mass ratio 3.0. The tests were carried out in a stepped current consisting of a uniform flow over the bottom 45% of the riser, while the remainder was in still water. The current was generated by towing the whole apparatus through water initially at rest, in five series of tests with different initial top tensions. Good quality results have been obtained on the frequencies and amplitudes of responses up to the 8th and 12th modes in transverse and in-line directions, respectively.

Our understanding of the measurements has benefited considerably from the fact that in one series of experiments a large number of tests was carried out at very small increments of velocity. This is very illuminating because the response

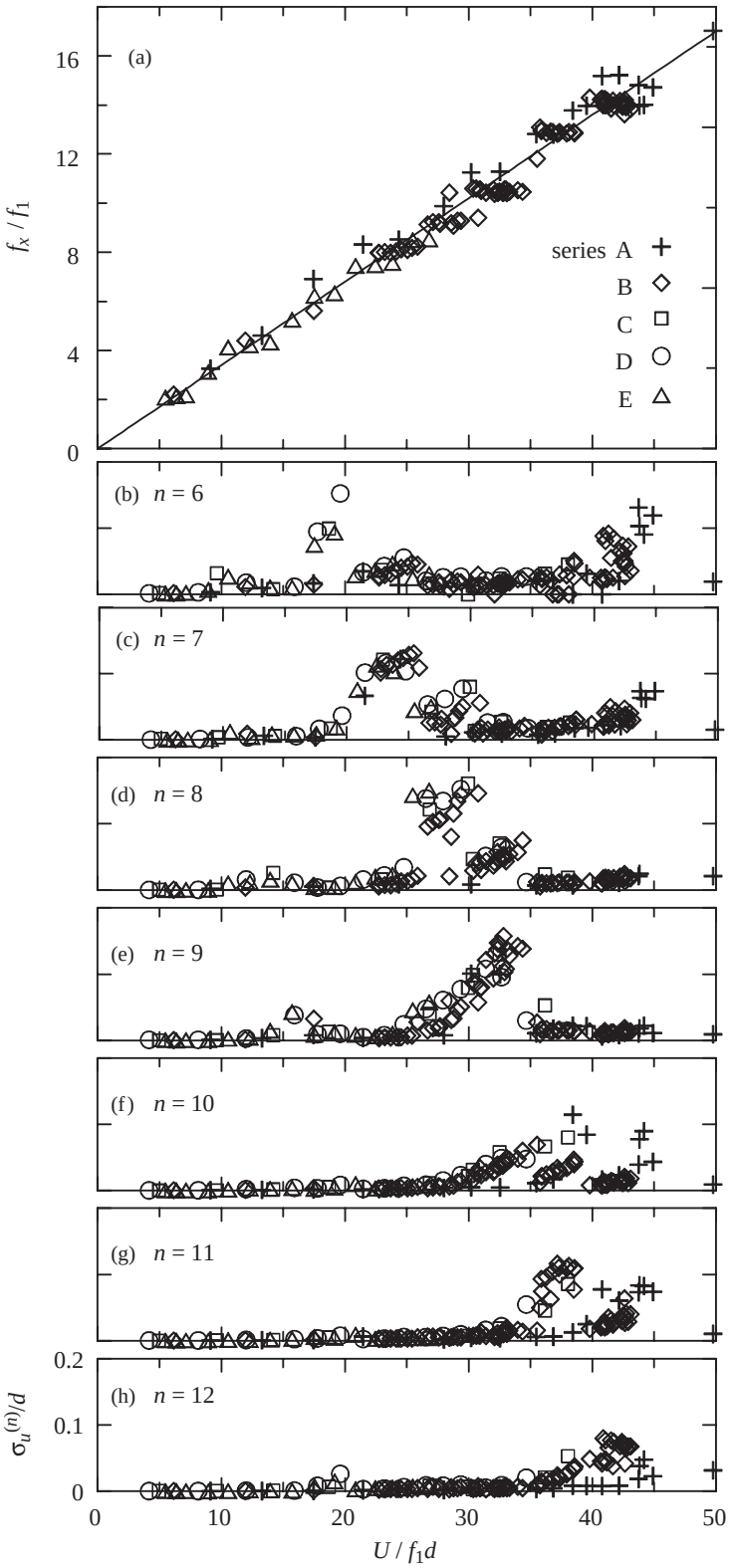

Fig. 15. Measurements of (a) in-line response frequencies and (b–h) standard deviations of in-line modal weights as functions of reduced velocity. A line in (a) indicates the double-Strouhal frequency corresponding to a Strouhal number of 0.17. All plots in (b–h) have identical scales. Data from all series are shown in (b–h); those from series C and D are omitted from (a).

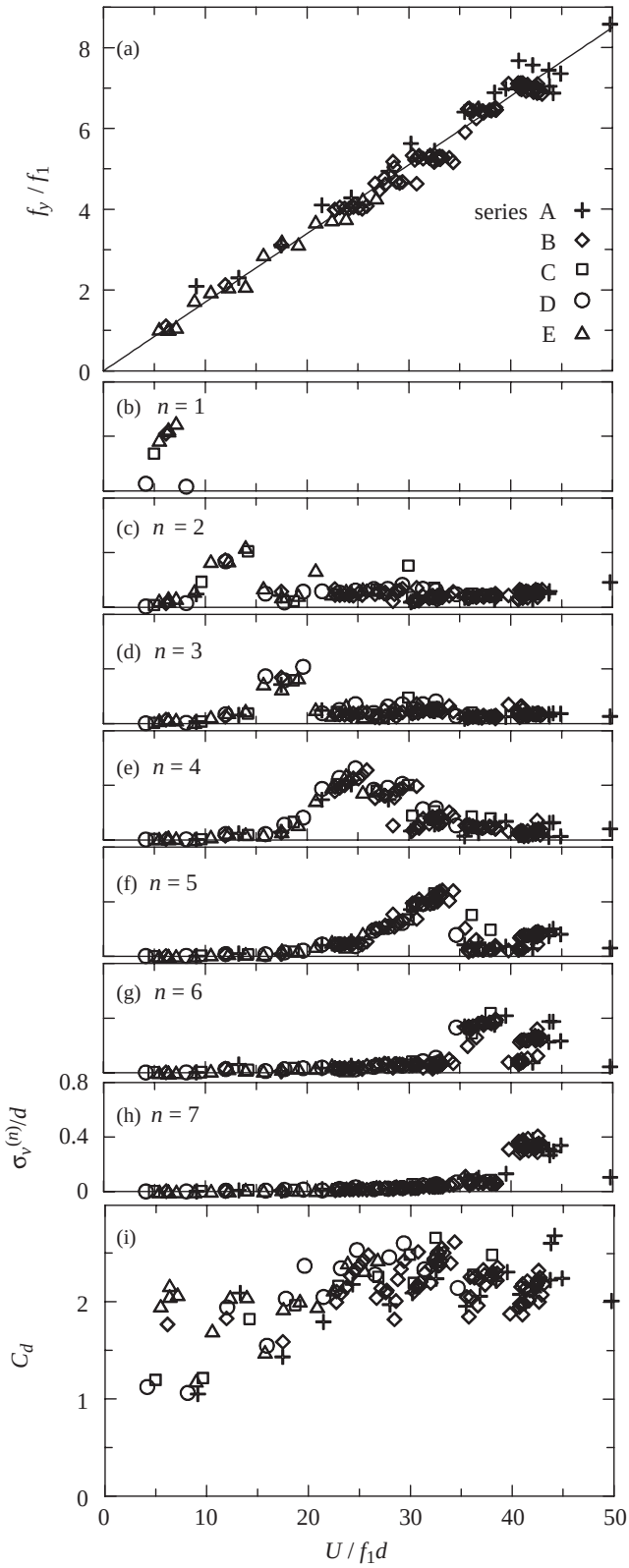

Fig. 16. Measurements of (a) cross-flow response frequencies, (b–h) standard deviations of cross-flow modal weights, and (i) drag coefficients as functions of reduced velocity. A line in (a) indicates the frequency corresponding to a Strouhal number of 0.17. All plots in (b–h) have identical scales. Data from all series are shown in (b–i); those from series C and D are omitted from (a).

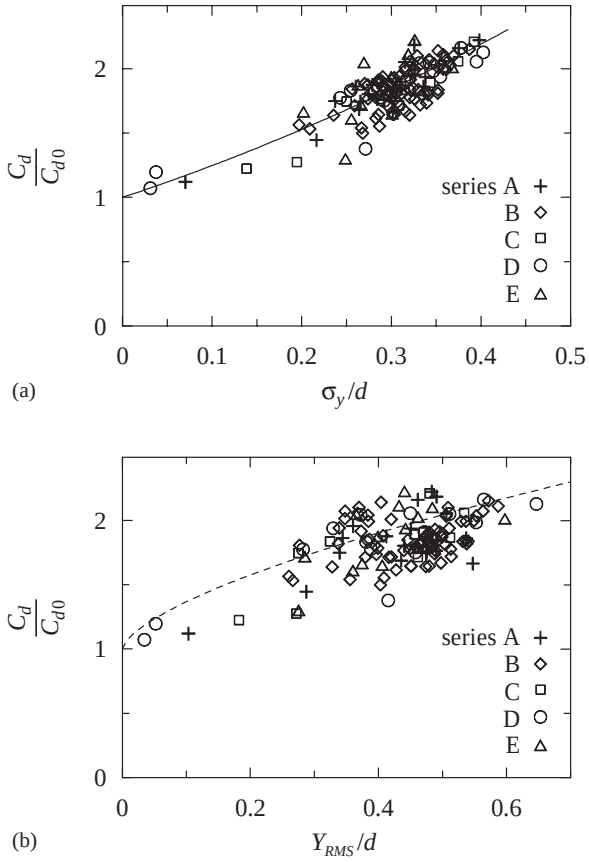

Fig. 17. Drag coefficients plotted as a function of (a) the overall standard deviation of cross-flow displacements (defined in Eq. (3)), and (b) the root-mean-square antinode displacement. The continuous line in (a) is $C_d/C_{d0} = 1 + 2.3\ (\sigma_y/d) + 1.7\ (\sigma_y/d)^2$; in (b) the broken line is $C_d/C_{d0} = 1 + 1.043(2Y_{\text{r.m.s.}}/d)^{0.65}$ (Vandiver, 1983). For each data point, C_{d0} is the drag coefficient for a stationary smooth cylinder in conditions of low free-stream turbulence at the same Reynolds number (Wieselsberger, 1921).

of the riser in amplitude and frequency (like the mean drag coefficient) was strongly correlated with the growth and attenuation of successive modes which, at high reduced velocities, occur at closely spaced intervals of velocity, with overlapping regions of excitation. For the purposes of this analysis the modes were identified with the spatial harmonics of the displaced profiles, without regard to the effects of changes in tension or added mass over the length of the riser. To understand the nature of the motion it was also helpful to segregate the data into intervals in which the modal composition of the response was essentially constant. The tests were of sufficient duration (up to 400 vortex-shedding cycles) for this to be possible, even though in some cases (particularly between modes) the excitation was found to be quite sensitive to external disturbances.

As the reduced velocity was increased, the dominant frequency of response advanced in distinct steps that marked in each case a switch from one dominant mode to the next. This strong lock-in behaviour also appears in results reported by King (1995) from tests with a cable vibrating in water with a mass ratio of 4.3. In the present case, the amplitude of the response in each mode grew monotonically as the reduced velocity increased through its lock-in range but then reduced, not smoothly but in one or two broken rising sequences, as the next mode became dominant. Generally the overall response of the riser included significant contributions from two or more modes, and each combination persisted over a range of reduced velocities. However, these ranges overlapped, so that a given reduced velocity could give rise to more than one pattern of modal contributions. The combined level of response increased steadily through each lock-in range, often to drop back sharply by 25% or more as a different combination of modes became established. These remarks apply equally to the in-line and cross-flow motions, and the steps in responses in both directions were clearly linked.

Standard deviations of individual modal weights reached 0.16 diameters in-line and 0.53 diameters cross-flow. Standard deviations of the combined response over time and over the length of the riser did not exceed 0.14 and 0.40 diameters, respectively. However, extreme single excursions of the riser went far beyond one diameter in the cross-flow direction and seemed to occur during a changeover in the modal composition of the response. In such less stable situations the motion of the lower part of the riser (in the current) was often dominated by a travelling wave. Generally, displacements in the upper part of the riser (in still water) were no less than in that part exposed to the current. Drag coefficients were correlated with the magnitude of the cross-flow response and exceeded those for a stationary smooth cylinder at the same Reynolds numbers by as much as 120%.

Acknowledgements

This work was supported by the EPSRC, by the European Commission though the MRI programme, and by BP.

Appendix A. Effect of large displacements of the riser on measured curvatures and displacements

In computing the deflected shape of the riser from measurements of curvature it was assumed that the effects of changes in the orientations of the strain gauges were insignificant. With the riser in an undeformed straight line condition the gauges that were installed to measure bending in the in-line direction x (the x-gauges) were on flat material faces parallel to the yz plane, and those designed to measure cross-flow curvature (the y-gauges) were on faces parallel to the xz plane. Departures from this alignment can be expressed in terms of the angles θ_x, θ_y in the horizontal plane between the normals to these material surfaces and the x and y directions, respectively. Clearly, large displacements of the riser could render each set of strain measurements subject to contamination due to bending in the orthogonal direction. A particular concern was that this effect could cause some small part of the large static in-line deflection to appear as a unsteady component at low modes in the measurements of cross-flow curvature.

The riser was very stiff in torsion and restrained in rotation at the bottom. Nevertheless, in the presence of large out-of-plane displacements, some twisting was inevitable owing to the elastic properties of the material. It must also be borne in mind that when the riser was displaced from the vertical in both xz and yz planes, the projections, in the horizontal plane, of normals to two orthogonal faces on it would no longer be orthogonal. The purpose of this appendix is to present the results of an analysis into the effect of these factors on computed displacements.

In order to find the effect of twist, the riser was modelled numerically using the ANSYS finite-element software package. This provided nonlinear solutions for the displacement of the riser when it was loaded statically to take up deformed shapes that were representative of extreme conditions observed in the experiments, with the same end conditions. In the example presented below, the loading consisted of steady drag in the in-line direction over that part of the riser that was exposed to the current, and a sinusoidal force distribution in the cross-flow direction. This was such as to produce a deflection of about one diameter in predominantly the 8th mode under an axial tension of 1000 N.

The projections in the xz and yz planes of the computed shape of the riser under these conditions are plotted as continuous lines in Figs. A1(a) and (b), with the accompanying material twist ϕ shown in Fig. A1(c). The misalignment angles θ_x, θ_y are plotted in Figs. A1(d) and (e). These do not exceed 0.6° and therefore have a negligible effect on the sensitivity of the x-gauges to in-line bending or on that of the y-gauges to cross-flow bending. What is of greater concern is the fact that in these conditions the y-gauges will register bending strains that are in fact due to the in-line curvature, with the consequence that, if uncorrected, this would lead to the appearance of a spurious displacement of the riser in the cross-flow direction. Its magnitude could be in the region of $\sin\theta_y$ times that in the in-line direction, in this case about 0.1 diameters, though it would also depend on the distribution of θ_y over the length of the riser. Its frequency in time would be the same as that of the actual cross-flow oscillation.

This effect was simulated by numerically generating the curvatures that would be measured by the strain gauges having been reorientated in accordance with the nonlinear finite element solution, and from these reconstructing the deflected shape of the riser by double integration in the usual way. The results are shown as broken lines in Figs. A1(a) and (b) and are almost indistinguishable from the originals. The modal weights u_n, v_n of the actual shape of the riser are set out in Table A1 for the first ten modes $1 \leqslant n \leqslant 10$, alongside those u'_n, v'_n that would be obtained from the uncorrected strain gauge readings.

As expected, the greatest effect of the misalignment of the gauges is in the first mode, but it amounts to no more than a change in amplitude of 0.03 and 0.02 diameters in the in-line and cross-flow directions, respectively. Bearing in mind that in the present context the case analysed here is a rather severe one, these results suggest that the rotation and

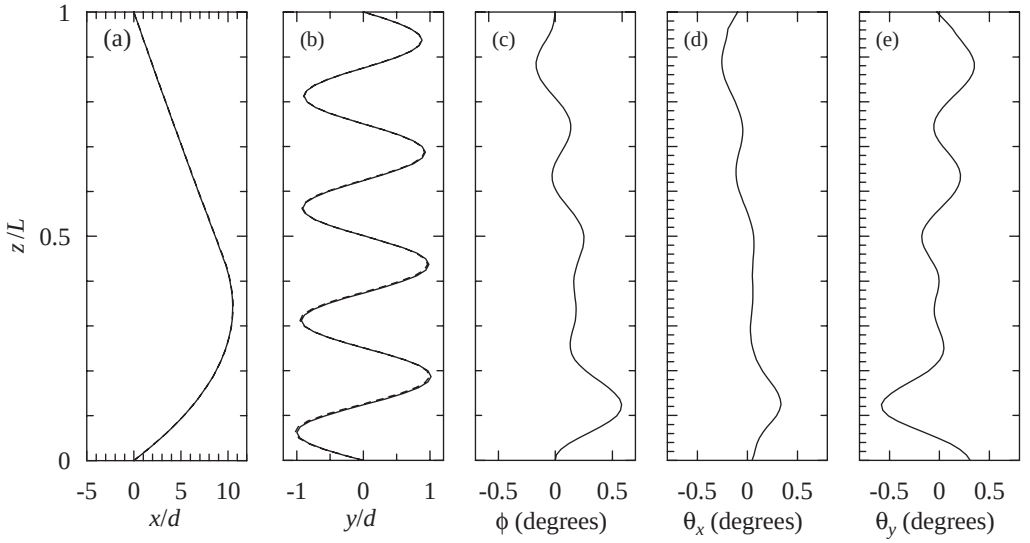

Fig. A1. Results of a simulation exercise on the effects of twist and misalignment of the strain gauges. Continuous lines in (a) and (b) show the actual deflected shape of the riser, and the corresponding twist is plotted in (c). The rotations of the gauges in the horizontal plane are shown in (d) and (e). Broken lines are plotted in (a) and (b) to show the shape of the riser that would be inferred from the displaced strain gauges, without correction.

Table A1
Modal weights u and v for the in-line and cross-flow directions respectively for the first 10 modes. Those with primes represent the values that would be obtained from the displaced strain gauges, without correction

n	u_n/d	u'_n/d	$(u'_n-u_n)/d$	v_n/d	v'_n/d	$(v'_n-v_n)/d$
1	9.33	9.35	0.03	0.03	0.01	−0.02
2	2.83	2.84	0.01	0.01	0.00	−0.01
3	0.64	0.64	0.00	0.00	−0.01	−0.01
4	0.06	0.06	0.00	0.00	−0.01	−0.01
5	0.03	0.03	0.00	−0.01	−0.01	−0.01
6	0.08	0.08	0.00	0.00	−0.01	−0.01
7	0.06	0.06	0.00	−0.03	−0.04	−0.01
8	0.02	0.02	0.00	−0.94	−0.94	0.00
9	0.00	0.00	0.00	−0.03	−0.02	0.00
10	0.01	0.01	0.00	0.00	0.00	0.00

displacement of the riser do not contribute significantly to uncertainties in modal weights computed directly from the strain gauge readings. The margins of error could however be much larger for model risers of greater length or curvature.

Appendix B. Data processing issues and uncertainties in computed modal weights

The magnitude of the bending strain associated with displacement of a given amplitude in the nth mode is proportional to n^2. This means that, when several modes are excited simultaneously, and displacements are computed from measured bending strains, the inferred contributions of the lowest modes will be subject to the greatest uncertainties.

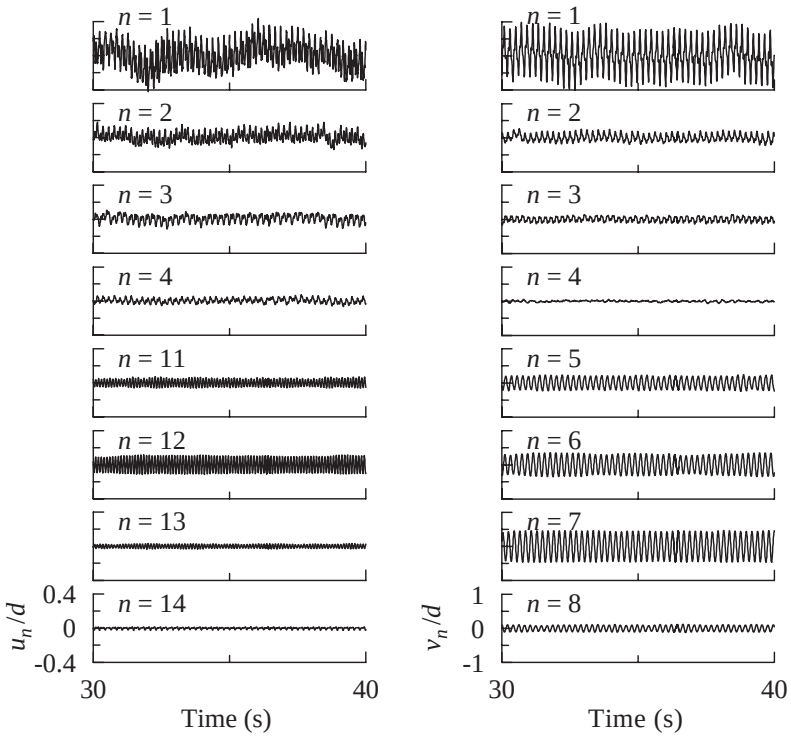

Fig. B1. In-line (left) and cross-flow (right) displacement modal weights for various mode numbers n, computed directly from the strain gauges. All plots in each column have the same scales. Velocity = 0.80 m/s, top tension = 877 N; case 21_A015.

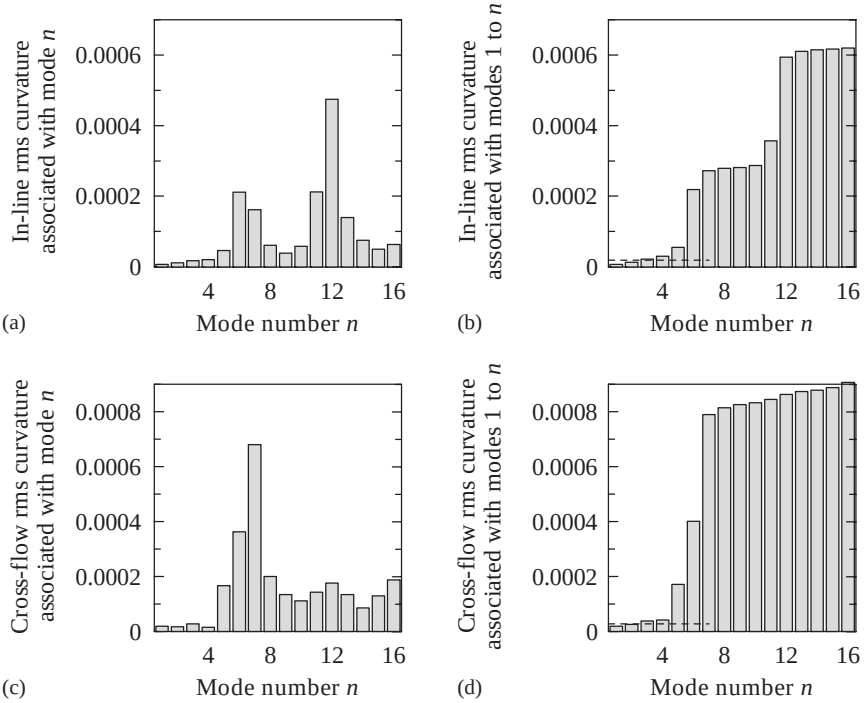

Fig. B2. Root-mean-square curvatures for the case shown in Fig. B1; (a) and (c) curvatures associated individual in-line and cross-flow modes, (b) and (d) curvatures associated with modes 1 to n. A broken line shows the 3% threshold.

Fig. B1 shows time series of in-line and cross-flow modal weights from a test at 0.80 m/s with a top tension of 877 N. These results were computed directly from the measured strains by double integration as described above, and reveal oscillations (amongst others) in the twelfth in-line mode and the 7th cross-flow mode. This is consistent with what might be expected of locked-in oscillations close to an appropriate Strouhal frequency. There are also oscillations in the first mode in both directions, and though these are of larger displacement amplitudes, the strains from which they were derived were very much smaller. This is seen in Figs. B2(a) and (c), which show the corresponding root-mean-square value of each mode in the measured curvatures. In the in-line direction the root-mean-square curvature in the first mode is less than 1.5% of that in the 12th; in the cross-flow direction the ratio between curvatures in the first and 7th modes is less than 3%. Figs. B2(b) and (d) show the curvatures associated with all modes up to the nth, as a function of n. As a proportion of the total curvatures, those associated with the first mode in each direction amount to less than 1.2% and 2.2%, respectively.

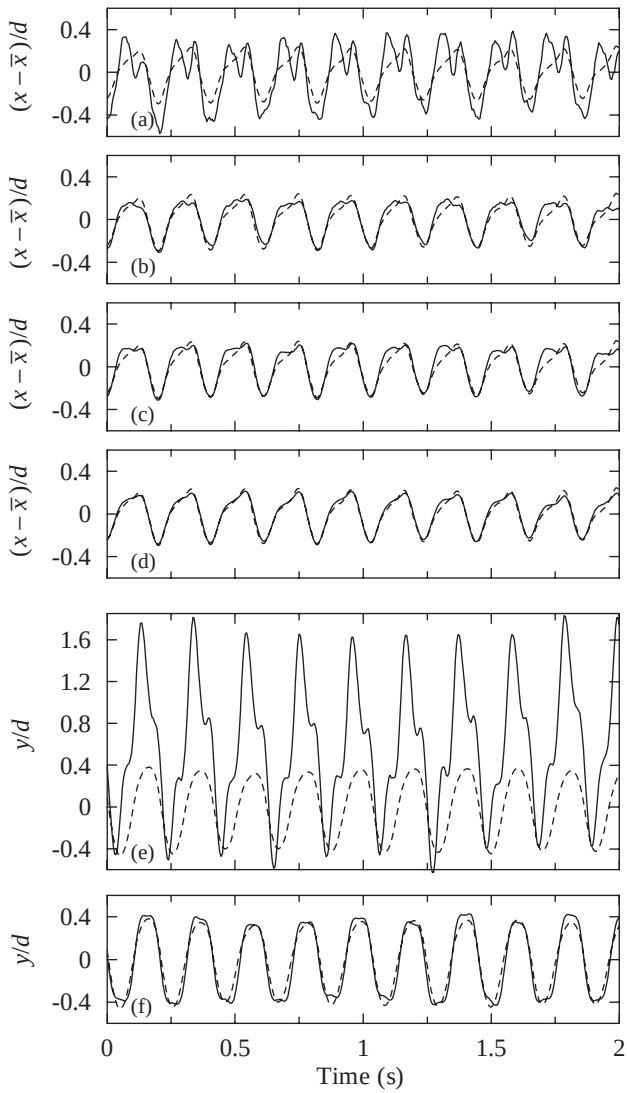

Fig. B3. Time series of displacements at the elevation of an accelerometer, $z = 5.65$ m, obtained from the accelerometer (broken lines) and strain gauges (continuous lines). Plots (a) and (e) show displacements obtained from the strain gauges without correction. Plots (b)–(d) show the effects of removing the first, second and third in-line modes from the strain gauge results, and (f) that of similarly removing the first cross-flow mode.

A level of uncertainty of around two percent in the measurements cannot be ruled out. Therefore, in cases such as that represented in Figs. B1 and B2 where two or more widely separated modes appear in the strain gauge results, the lowest ones must be treated with considerable caution. Independent measurements of displacements were available from the accelerometers placed at two points within the riser, and in processing the strain gauge data we adopted the following procedure. First, the fundamental mode of displacement in each direction was excluded from the analysis when the root-mean-square curvature associated with it was less than 3% of that of all computed modes. This cut-off level is shown in Figs. B2(b) and (d). In almost all cases this brought the computed cross-flow motion at the elevations of the accelerometers into excellent agreement with displacements inferred from the measured accelerations. However, in the in-line direction there was much greater potential for any contamination to reach beyond the fundamental, owing to the fact that in this direction the dominant modes of displacement were about twice as high. Therefore in a second stage of processing, the lowest remaining modal contributions were progressively removed from the strain gauge results until the displacements computed from them were in agreement with those obtained from acceleration measurements.

To illustrate this process, Fig. B3 compares in-line and cross-flow displacements obtained from the strain gauges (continuous lines) and accelerometers (broken lines) for the same test case. In Figs. B3(a) and (e) the strain gauge results are shown before the correction procedure described above had been applied. In the cross-flow direction the removal of the first mode from the strain gauge results (Fig. B3(f)) achieves much better agreement with the acceleration measurements, while in the in-line direction a comparable match is reached only after the contributions of the first three modes have been taken out. This exercise was repeated for all test cases.

An alternative to this problem, based on an a priori selection of modes that are likely to be present, is proposed by Lie and Kaasen (2004).

References

Chaplin, J.R., Bearman, P.W., Huera Huarte, F.J., Pattenden, R.J., 2004a. Laboratory measurements of vortex-induced vibrations of a vertical tension riser in a stepped current. In: de Langre, E., Axisa, F. (Eds.), Proceedings of the Eigth International Conference on Flow-Induced Vibration, vol. 2, Paris, France, pp. 279–284.

Chaplin, J.R., Bearman, P.W., Fontaine, E., Herfjord, M., Isherwood, M., Larsen, C.M., Meneghini, J.R., Moe, G., Triantafyllou, M.S., 2004b. Blind predictions of laboratory measurements of vortex-induced vibrations of a tension riser. In: de Langre, E., Axisa, F., (Eds.), Proceedings of the Eighth International Conference on Flow-Induced Vibration, vol. 2, Paris, France, pp. 285–290.

Chaplin, J.R., Bearman, P.W., Cheng, Y., Fontaine, E., Graham, J.M.R., Herfjord, M., Isherwood, M., Lambrakos, K., Larsen, C.M., Meneghini, J.R., Moe, G., Triantafyllou, M.S., Willden, R.H.J., 2005. Blind predictions of laboratory measurements of vortex-induced vibrations of a tension riser. Journal of Fluids and Structures 21, 25–40.

Johanning, L., Bearman, P.W., Graham, J.M.R., 2001. Hydrodynamic damping of a large scale surface piercing circular cylinder in planar oscillatory motion. Journal of Fluids and Structures 15, 891–908.

King, R., 1995. An investigation of vortex induced vibrations of sub-sea communications cables. In: Bearman, P.W. (Ed.), Proceedings of the Sixth International Conference on Flow Induced Vibrations, London, UK, pp. 443–454.

Lie, H., Kaasen, K.E., 2004. Private communication.

Lie, H., Larsen, C.M., Vandiver, J.K., 1997. Vortex induced vibrations of long marine risers; model test in a rotating rig. In: Chakrabarti, S., Kinoshite, T., Maeda, H., Ertekin, C. (Eds.), Proceedings of the 16th International Offshore Mechanics and Arctic Engineering Conference, vol. I-B. ASME, Yokohama, pp. 241–252.

Lie, H., Mo, K., Vandiver, J.K., 1998. VIV model of a bare- and a staggered buoyancy riser in a rotating rig. Offshore Technology Conference OTC No. 8700, Houston, TX, USA.

Sarpkaya, T., 2004. A critical review of the intrinsic nature of vortex-induced vibrations. Journal of Fluids and Structures 19, 389–447.

Vandiver, K., 1983. Drag coefficients of long flexible cylinders. Offshore Technology Conference OTC No. 4490, Houston, TX, USA.

Wieselsberger, C., 1921. Neuere festellungen über die Gesetze des Flüssigkeits und Luftwider-standes. Physikalische Zeitschrift 22, 321–328.